Mesoporous Silicates

DOI: 10.1002/ange.200500113

Synthesis of Mesocage Structures by Kinetic Control of Self-Assembly in Anionic Surfactants**

Alfonso E. Garcia-Bennett, Natalia Kupferschmidt, Yasuhiro Sakamoto, Shunai Che, and Osamu Terasaki*

Molecular self-organization is the topic of numerous fundamental and applied studies for its potential in diverse applications in areas ranging from catalysis to photonic crystals, from biomimetic chemistry to sensor technology.[1–3] The study of such systems is central to physics, mathematics, biological systems, and materials chemistry alike. Innovative methods for the assembly of ordered structures with self-assembling building units at various length scales are constantly proposed. Among these, the self-assembly of lyotropic liquid crystals to form mesoporous structures, as pioneered by Kresge et al.,[4] is the center of a large academic and industrial effort due to the high potential to tailor porous properties of high-surface-area inorganic frameworks through variations in the self-assembling surfactant template and synthesis conditions. Functionalization of their internal surfaces renders them suitable for applications. New synthetic methods for the preparation of mesoporous structures are being developed. For example, the enlargement of pore sizes by the use of polymeric surfactants has led to mesoporous solids with enhanced diffusion and transport properties such as SBA-15 (*p6mm*), FDU-5 ($Ia\bar{3}d$), and SBA-16 ($Im\bar{3}m$).[5,6] Low-symmetry mesostructures have been reported previously, obtained using bolaform surfactants, as in the case of two-

[*] Dr. A. E. Garcia-Bennett, N. Kupferschmidt, Dr. Y. Sakamoto, Prof. O. Terasaki
Structural Chemistry, Arrhenius Laboratory
Stockholm University
10691 Stockholm (Sweden)
Fax: (+46) 8-163-118
E-mail: alf@struc.su.se
Prof. S. Che
Department of Chemistry
School of Chemistry and Chemical Technology
Shanghai Jiao Tong University
800 Dongchuan Road, Shanghai, 200240 (P. R. China)

[**] We are grateful to Dr. Bodo Zibrowius and Prof. Ferdi Schüth (Max-Planck-Institut für Kohlenforschung, Mülheim) for conducting NMR experiments and for helpful discussions, and to AminoScience Lab, Ajinomoto Co., Inc., for providing *N*-lauroyl glutamic acid. A.E.G.-B. is grateful to the European Research and Training Network "Nanocage Materials" for funding (grant no. HPRN-CT-2002-00193). This work was partly supported by the Swedish Science Council (VR) and by Core Research for Evolutional Science and Technology (CREST) of JST and BNRI, Japan (O.T.). The authors are grateful to Q. Chen (East China Normal University) for additional NMR experiments.

Supporting information for this article is available on the WWW under http://www.angewandte.org or from the author.

dimensional SBA-8 (*c2mm*),[7] and by evaporation-induced self-assembly (EISA).[8,9]

Recently, the preparation of highly ordered mesoporous structures using anionic surfactants and co-structure-directing agents (CSDAs) was reported.[10] This synthesis route has proven successful for the formation of several novel mesoporous phases. A face-centered cubic structure ($Fd\bar{3}m$), named anionic mesoporous solid (AMS-*n*) AMS-8, was identified and modeled by electron crystallography.[11] Furthermore, a hexagonal structure with chiral arrangement of the pores has been prepared.[12] The diversity of structure types that are possible using *N*-acyl amino acid anionic surfactants is already impressive, but little is known about the interaction of the CSDA with the anionic head group of the surfactant and its role in the synthesis mechanism.

A third structure, formed by the use of *N*-lauroyl glutamic acid as anionic surfactant and (3-aminopropyl)trimethoxysilane (APS) as CSDA, has been proposed. Named AMS-2, this mesocage silicate is composed of nonperiodic structural modulations observable as unit cell shifts of one-half.[13] Spherical micelles, which are used as templates for mesocage solids such as AMS-2, form in lipid/water and surfactant systems and undergo thermal, compositional, and time-dependent kinetically controlled structural transformations. Transitions can be described in terms of the surfactant packing parameter *g*, which is dependent on the kinetic surfactant chain length, the effective head-group area at the micelle surface, and the total surfactant volume. In practice, few phases are observed and it is difficult to control kinetics in structural transformations.[14]

Herein we demonstrate the possibility of inducing structural transformations in the synthesis of mesocage materials by delaying the time of addition of the silica source (tetraethyl orthosilicate, TEOS) with respect to the CSDA, the importance of which is clearly associated with precise control of the micellar (local) and structural (mesoscale) characteristics of the resulting porous solid.

A phase transformation expanding four different cubic structures was studied. Powder X-ray diffraction (XRD) data are unable to yield detailed structural information despite the increased order of AMS-*n* mesostructures. In contrast, electron microscopy investigations clearly show that it is possible to form mesoporous structures of lower symmetry with counterparts in atomic-scale materials such as intermetallic compounds.

These investigations open up avenues in synthesis, characterization, and application that are central to the development not only of mesoporous structured materials but also nanotechnology and materials engineering.

Figure 1 shows high-resolution transmission electron microscopy (HRTEM) images recorded along high-symmetry zone axes of calcined mesostructures synthesized with different APES-*t*-TEOS, for which *t* denotes the time in minutes between the addition of the CSDA and TEOS, *N*-lauroyl glutamic acid as self-assembling anionic surfactant, and aminopropyltriethoxysilane (APES) as CSDA. Tilt-series selected-area electron diffraction (SAED) patterns were recorded to determine the structural characteristics of each sample and confirmed the presence of four separate meso-

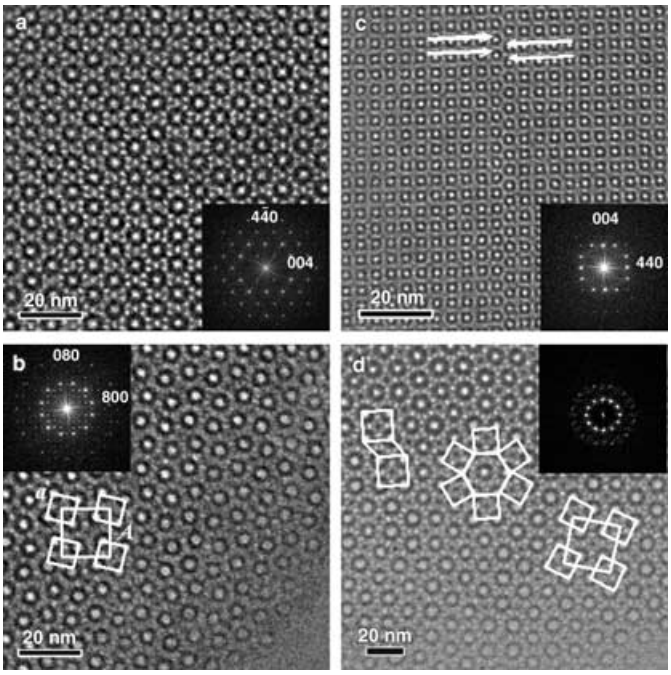

Figure 1. HRTEM images of mesocage structures synthesized by using *N*-lauroyl glutamic acid as surfactant and APES as CSDA. Images are viewed along a) [110] (AMS-8, $Fd\bar{3}m$), b) [001] (AMS-9, $P4_2/mnm$), c) [100] (SBA-1-type, $Pm\bar{3}n$), and d) (AMS-2; modulated structure). White insets show the periodic zigzag arrangement of cages in AMS-9 and the resulting superlattice, where $a = 84$ and $A = 168$ Å (b), and the nonperiodic arrangement of domains in AMS-2, composed of two distinct units, namely, slabs of $Pm\bar{3}n$ and $P4_2/mnm$ structures, as well as other motives and defects of the stacking-fault type (d). The insets show in all cases corresponding Fourier transform diffractograms.

structures in the *N*-lauroyl glutamic acid/APES system reported here. All samples display a high degree of periodicity over large areas and stability under the electron beam. Figure 1 a shows an HRTEM image recorded along the [110] orientation of APES-0-TEOS. Electron microscopy investigations are consistent with a cubic structure, and extinction conditions allow the space group symmetry to be confirmed as $Fd\bar{3}m$.

At first instance it is possible to deduce a lattice unit based on a cubic unit cell ($Pm\bar{3}n$) with $a = 84.0$ Å for a calcined sample of APES-2-TEOS (Figure 1 b). Periodic stacking faults characterized by unit cell shifts of one-half are clearly observed. The faults are arranged regularly to form a 2D antiphase boundary. From this image and the corresponding diffraction pattern a superlattice unit cell is easily determined, as outlined in Figure 1 b (inset). From a series of HRTEM tilt-series images and diffraction patterns it is possible to determine the crystal class and unit cell lattice parameters. The new superstructure is tetragonal, with lattice constants $(A)a = 167.9$ and $c = 84.0$ Å. This novel structure has been named AMS-9 (anionic surfactant-templated mesoporous silica 9). The formation of similar superstructures from cubic phases is well documented for intermetallic compounds and liquid crystals.[15,16] This strongly suggests that the formation of lower-symmetry 3D structures can be achieved at the mesoscale.

Figure 2 shows SAED patterns recorded along the [001], [110], [101], and [111] directions of AMS-9. The unusually numerous reflection spots at higher scattering angles in comparison with other mesoporous materials indicate a highly ordered mesostructure and a sharp density boundary between cage cavity and wall. Observable reflections can be summarized with the following general conditions: hkl, $hk0$, hhl, $hh0$: no condition, $0kl$: $k+l=2n$, $00l$: $l=2n$, $0k0$: $k=2n$, reducing the possible space-group symmetry to $P4_2nm$, $P\bar{4}n2$, or $P4_2/mnm$. The latter was chosen for its highest symmetry.

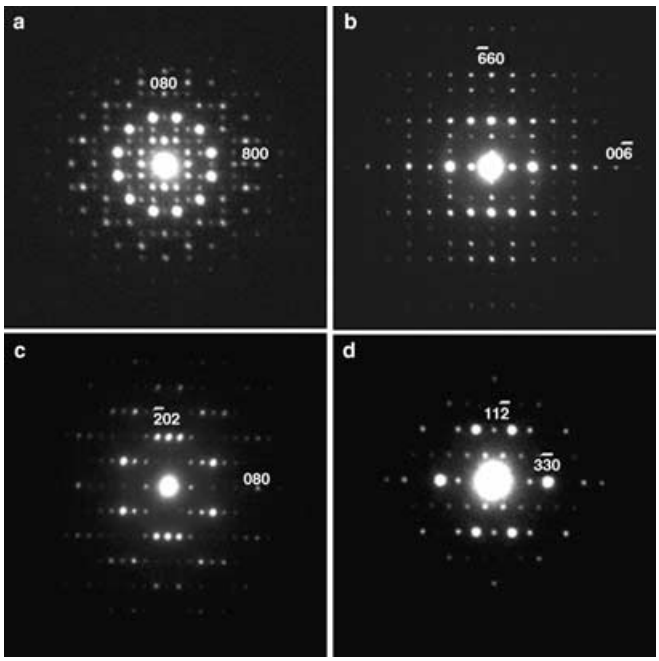

Figure 2. SAED patterns of calcined AMS-9 recorded along a) [001], b) [110], c) [101], and (d) [111] directions. Patterns are indexed on the basis of a tetragonal unit cell with lattice constants $a=167.9$ and $c=84.0$ Å. Reflection conditions are consistent with the space-group symmetry $P4_2/mnm$.

A 3D reconstruction of the structure,[17] based on analysis of Fourier transform (FT) diffractograms taken from thin parts of crystals (see Supporting Information), along high-symmetry zone axes of AMS-9 was conducted. Phase and amplitude of the structure factors were extracted from the 16 strongest reflections. Amplitudes were normalized by using common reflections obtained from images along [001], [101], [111], and [110] orientations. However, a unique set of phases could not be extracted from these four images due to the small number of common reflections encountered in tetragonal systems along these directions. The most probable data set (see Supporting Information) out of four possibilities can be deduced by considering neighboring cubic cage-type structures $Pm\bar{3}n$ and $Fd\bar{3}m$. From electrostatic potential density maps, it follows that cages in AMS-9 are arranged with space group $P4_2/mnm$. Figure 3a shows three 2D-sliced electrostatic potential density maps of the unit cell of AMS-9.

To obtain quantitative data about cage size and connectivity between cages from reconstructed data, an accurate estimation of the contrast transfer function (CTF) must be conducted. Almost all strong reflections of AMS-9 are at higher scattering angles than those of other mesoporous materials, so the relative intensity of each reflection is more sensitive to the CTF correction. A tentative model of the cage arrangement can be constructed based on $Pm\bar{3}n$ structural units (Figure 3b). The unit cell of AMS-9 is composed of 30 cages. Further analysis is being conducted to determine the size and connectivity of cages, and our findings will be reported shortly.

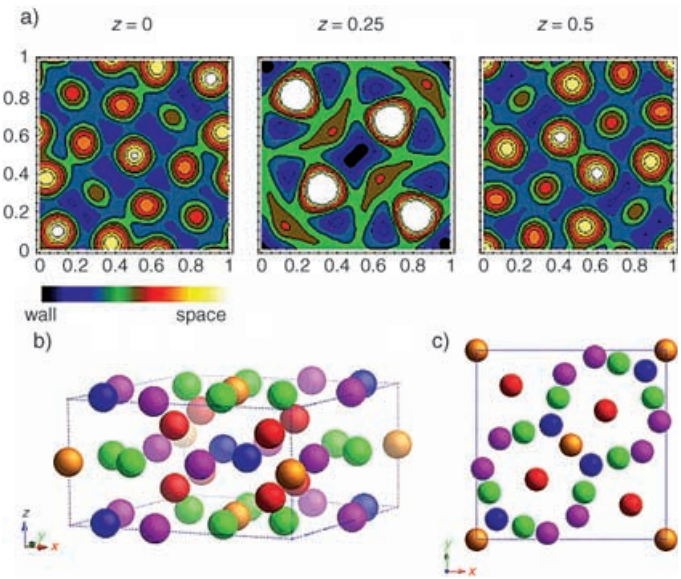

Figure 3. a) 2D electrostatic potential density maps derived from electron microscopy of the unit cell of AMS-9, shown parallel to the [001] plane. The unit cell slices are taken with $z=0$, 0.25, and 0.5. White contrast represents the pore space, and black contrast the silica wall. b), c) Model of the packing arrangement of cages in AMS-9, based on a $Pm\bar{3}n$ unit cell containing 30 cages (b), and viewed along the [001] direction (c). Each color represents a different crystallographic site of $P4_2/mnm$.

Samples synthesized in the range APES-6 $<t>$ 9-TEOS showed modulated structures that often contained a large number of defects of the stacking-fault type. Figure 1d shows a typical HRTEM image recorded on AMS-2 (APES-6-TEOS). Two structural units can be observed, based on $Pm\bar{3}n$ and $P4_2/mnm$ mesocage solids AMS-9 and SBA-1, in addition to stacking faults and motives showing the typical arrangement of cages.

A transition with time following the sequence $Fd\bar{3}m \rightarrow P4_2/mnm \rightarrow Pm\bar{3}n \rightarrow$ modulated structure $\rightarrow Fd\bar{3}m$ is observed when materials are prepared at 60 °C in the range APES-0 $<t>$ 10-TEOS. All structures obtained are mesocage materials. The apparent return to $Fd\bar{3}m$ is not fully understood. The proximity of all four structures in the phase diagram of *N*-lauroyl glutamic acid is a representation of the small differences in stabilization energy between each structure type. It is evident that small changes in the local environment of the spherical micelles caused by interaction and hydrolysis of the CSDA have a pronounced effect on the overall packing arrangement of the micelle. Similar structural transitions have been observed in systems using *N*-lauroyl glycine, lauric acid, and pluronics as surfactants, and APS, *N*-trimethoxysilyl-

propyl-*N*,*N*,*N*-trimethylammonium chloride (TMAPS), and (3-mercaptopropyl)triethoxysilane (MPTS)[18] as CSDAs.

Mesostructures with $Fd\bar{3}m$ and $Pm\bar{3}n$ space-group symmetries have been reported previously,[11,16] and are the subject of continued structural and applied research as a result of their intricate 3D network of mesocages, connected to each other by small (< 20 Å) pore windows which can be used for the entrapment of functional guests such as dyes, metal oxides, or metal centers. The unit cell parameters for each of these structures as derived from TEM data are $a =$ 162.6 and $a = 82.8$ Å for the $Fd\bar{3}m$ and $Pm\bar{3}n$ phases, respectively. Both $Fd\bar{3}m$ (named AMS-8) and $Pm\bar{3}n$ (SBA-1-type) mesostructures (Figure 1a and c) are formed by self-assembly and cubic packing of spherical or pseudospherical micelles of different sizes. In the case of AMS-2 and AMS-9, the formation of new types of spherical cages is evident from electron microscopy. Evidence of a transition mechanism based on stacking faults can be clearly observed by electron microscopy (see Supporting Information). The connectivity and pore arrangement of intermediate phases are expected to be considerably different from samples that show no structural defects.

The structural and porous characteristics of samples reported here are summarized in Table 1. Raw-data nitrogen adsorption isotherms and pore size distribution curves are shown in the Supporting Information. From the capillary condensation steps it is possible to identify a structural change in samples synthesized with different APES-*t*-TEOS. An extra step is observed in the capillary condensation region of AMS-8, owing to a significant difference in cage size between its larger cage (44.5 Å) and smaller cage (40.3 Å). The adsorption curves of cubic structures SBA-1 and AMS-9 follow similar adsorption/desorption paths and show no hysteresis in the desorption branch; this indicates similarities in the packing arrangement of these two structures. However AMS-9 shows a higher total pore volume and a slight shift to higher pressures owing to the presence of larger cages. The modulated structure of AMS-2 shows decreased adsorption capacity and a smaller cage size. In this modulated structure it is possible that cages may be blocked to the external surface of the mesoporous particles, as a darkening of this sample is observed after calcination of the surfactant. Pore size distribution curves for all structures show additional peaks centered around 10 Å. These can be assigned to adsorption in the small connecting channels between cages.

The ^{29}Si MAS NMR spectra of calcined and extracted samples of AMS-9 are shown in Figure 4. The presence of T^3 and T^2 peaks between 50 and 65 ppm, attributed to $(R)Si(OSi)_3$ and $R(HO)Si(OSi)_2$, respectively, in the ^{29}Si MAS NMR spectra of a solvent-extracted sample of AMS-9 is evidence for the functionalization of the amorphous silicate framework with aminopropylsilane groups. The T^n/Q^n ratio of the as-synthesized (4.6:1) and extracted samples (3.2:1) of AMS-9 both indicate high incorporation of the CSDA. The data obtained by deconvolution agree well with the ratios derived from the integrals. This constitutes a direct method for incorporation of organic functional groups and offers considerable advantages for further functionalization of mesoporous structures over grafting and post-synthetic treatments.[19]

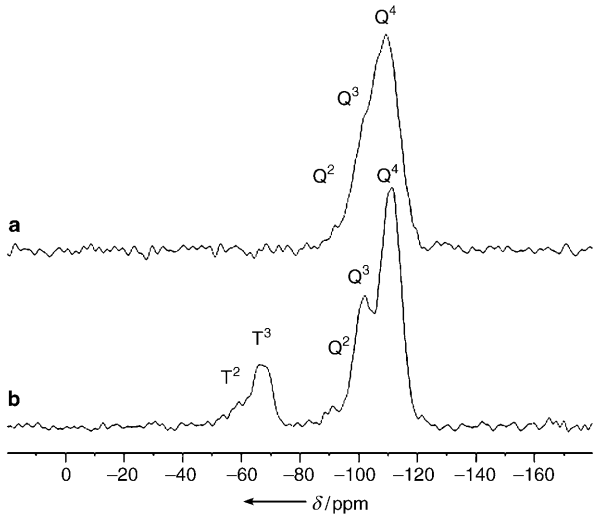

Figure 4. ^{29}Si CP-MAS NMR spectrum of calcined AMS-9 (a), and ^{29}Si MAS NMR spectrum of an extracted sample of AMS-9 (b). Peaks at $\delta = -92$, -100, and -109 ppm are attributed to Q^2, Q^3,and Q^4 silicon atoms ($Q^n = Si(OSi)_n(OH)_{4-n}$). T^3 and T^2 peaks can be attributed to $(R)Si(OSi)_3$ and $R(HO)Si(OSi)_2$, respectively.

Table 1: Structural and porous characteristics of mesocage solids synthesized with different APES-*t*-TEOS.

APES-*t*-TEOS (min)	Mesostructure (space group)	Unit cell parameter (TEM) [Å]	Unit cell parameter (XRD) [Å]	Pore size (DFT) [Å]	Total pore volume [cm^3g^{-1}]	Surface area [m^2g^{-1}]
0	3D cubic ($Fd\bar{3}m$)	162.6	154.9	42.4 40.2	0.58	755.3
2	3D tetragonal ($P4_2/mnm$)	167.9 (*c*) 84.0 (*a*)	172.0 (*c*) 90.2 (*a*)	38.3	0.60	872.2
4	3D cubic ($Pm\bar{3}n$)	88.8	94.8	36.0	0.58	890.4
6	modulated structure			34.2	0.43	710.0
10	3D cubic ($Fd\bar{3}m$)	145.6	152.5	44.5 40.3	0.59	724.5

Figure 5 shows XRD patterns of a structural transformation in the AMS-2 system induced by delaying addition of the silica source from 0 to 10 min (APES-*t*-TEOS). Clear structural transformations are observed. The XRD patterns obtained at APES-0-TEOS and APES-10-TEOS show similar diffraction peaks that can be indexed on the basis of a cubic unit cell with space group symmetry $Fd\bar{3}m$ with unit cell lattice constants of 154.9 and 152.5 Å for APES-0-TEOS and APES-10-TEOS, respectively. It is not possible to derive structural information directly from the XRD of samples prepared in the range APES-1-TEOS to APES-9-TEOS due

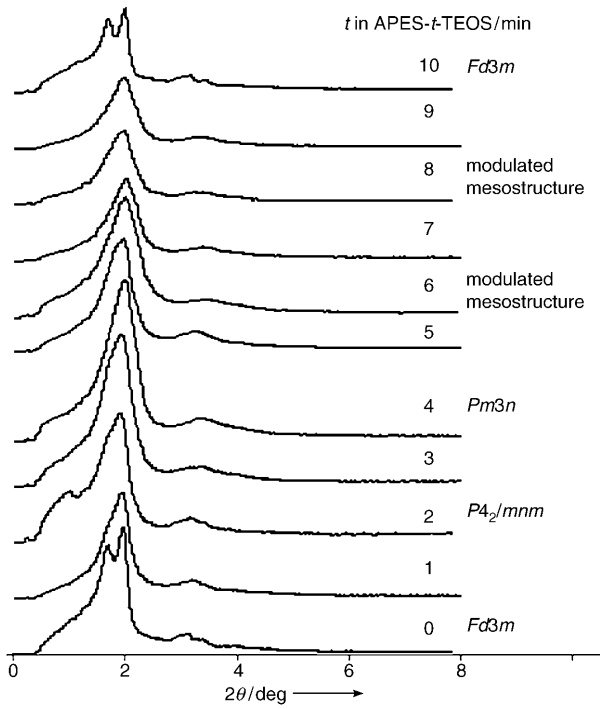

Figure 5. XRD patterns of calcined samples of mesostrucures synthesized by variation of the time of addition of the silica source with respect to the CSDA (APES-*t*-TEOS).

to the proximity of diffraction peaks at low scattering angles and the various defects associated with each structure. A typical example is the case of the $P4_2/mnm$ structure (APES-2-TEOS), where both SAED patterns show many very sharp reflections at low scattering angle.

In the system described herein the interaction between the CSDA and the hydrophilic head group of the anionic surfactant governs the phase transformation and allows control of the structural features of the desired phase. This might be due to an increase in the hydrophobicity at the interface between the surfactant head group and the CSDA. The use of organoalkoxysilanes has been noted to cause a stabilization of the structural properties of the resulting silicate products.[19] The rate of hydrolysis of the organoalkoxysilane (APES) is considerably slower than that of the tetraalkoxysilane (TEOS) due to the presence of the organic group bonded to Si. The addition of the latter allows the stabilizing anionic surfactant/CSDA micelle to "freeze" prior to condensation of the framework.

Bimodal spherical micelles are formed in this system in a ratio that varies considerably as the CSDA is hydrolyzed and interacts electrostatically with the surfactant head group, forcing the micellar interface to undergo conformational changes in shape and size. The possibility to study these changes through silicate intermediate phases offers the potential to control not only the structure but also the cage shape and connectivity with increased accuracy. This has been demonstrated by use of a CSDA to form a new structure, named AMS-9 ($P4_2/mnm$).

Analysis by HRTEM and fast Fourier transform (FFT) clearly shows the evolution with time of the CSDA effect. Ordered structures with long-range order are observed, in contrast to XRD evidence that reveals broad diffraction peaks suggesting disordered pore structures.

A fast and simple method with potential to form new structures, to design the extent of defects and size and shape of mesocages, and to functionalize the internal surface of mesoporous materials has been described. This approach has been applied in different anionic surfactant/CSDA systems and is largely extendable to different interactions by charge matching with the corresponding CSDA. Further synthetic and structural studies are being conducted and will be reported shortly.

Experimental Section

In a typical synthesis 0.2 g of *N*-lauroyl L-glutamic acid (C_{12}GlutA) was dissolved in 20 mL of deionized water with stirring at 80 °C overnight. The solution was cooled to 60 °C before 0.36 g of APES was added with rapid stirring (300 rpm). Tetraethyl orthosilicate (TEOS, 1.5 g) was added after a period of between 0 and 10 min (APES-*t*-TEOS) to give a final TEOS/APES/C_{12}GlutA/H_2O molar ratio in the gel of 1:0.21:0.085:154.

The pH value of the starting surfactant solution was 3.54 and rose rapidly to 9.30 (within seconds) on addition of the CSDA. The pH value of the reaction gel was 9.30 prior to the addition of TEOS. The pK_a values for the carboxylate groups in C_{12}GlutA were estimated on the basis of data for the free amino acid to be 2.19 and 4.25, while the isoelectronic point is 3.22. This implies that under the conditions of synthesis a strong electrostatic interaction between the surfactant head group and the CSDA is expected. The resultant silica gel solution was stirred for 10 min at 60 °C to promote hydrolysis of the CSDA and the silicate precursor. The reaction gel was then allowed to stand at 60 °C for 1 d with no stirring and for a further 2 days at 100 °C. After the reaction was complete the precipitate was collected by filtration, washed with 100 mL of H_2O, and dried overnight at room temperature. The surfactant was removed by calcination at 550 °C (1 h in flowing N_2, then 6 h in O_2) to give the porous AMS-*n* silicates. Alternatively, the surfactant was removed by solvent extraction in a Soxhlet apparatus with ethanol for 3 days.

XRD patterns were recorded on an STOE powder diffractometer equipped with $Cu_{K\alpha}$ radiation (40 kV, 20 mA) at a rate of 1.0 deg min^{-1} over the range of 1.0 to 10.0°.

The N_2 adsorption/desorption isotherms were measured at −196 °C on an ASAP 2020 Micromeritics Instrument. Calcined mesoporous AMS-*n* was outgassed for 6 h at 200 °C and 0.3 kPa. The BET specific surface area was evaluated from the adsorption data in the relative pressure range from 0.05 to 0.3. The total pore volume was estimated from the amount adsorbed at a relative pressure of 0.96. Pore size distribution curves were derived by NLDFT by assuming a spherical model of cages.

TEM was carried out with a JEOL JEM-3010 microscope operating at 300 kV ($C_s = 0.6$ mm, resolution 1.7 Å). Images were recorded with a CCD camera (model Keen View, SIS analysis, 1024 × 1024 pixels, pixel size 23.5 × 23.5 μm) at 30000–100000 × magnification under low-dose conditions.

^{29}Si MAS NMR spectra were measured on a Bruker Avance 500WB spectrometer with a 4-mm MAS probe under the following experimental conditions: 2.2 μs π/4 pulses, 30 s recycle delay, 2400 scans, and a spinning rate of 10 kHz.

Received: January 12, 2005
Revised: May 19, 2005
Published online: July 20, 2005

Keywords: electron diffraction · electron microscopy · mesoporous materials · silicates · surfactants

[1] R. Vargas, P. Mariani, A. Gulik, V. Luzzati, *J. Mol. Biol.* **1992**, *225*, 137 – 145.
[2] N. Khazanovich, J. R. Granja, D. E. McRee, R. A. Milligan, M. R. Ghadiri, *J. Am. Chem. Soc.* **1994**, *116*, 6011 – 6012.
[3] E. A. Lord, A. L. Mackay, *Curr. Sci.* **2003**,*7*, 346 – 362.
[4] C. T. Kresge, M. E. Leonowicz, W. J. Roth, J. C. Vartuli, J. S. Beck, *Nature* **1992**, *359*, 710 – 712.
[5] D. Y. Zhao, J. Feng, Q. Huo, N. Melosh, G. H. Fredrickson, B. F. Chmelka, G. D. Stucky, *Science* **1998**, *279*, 548 – 552.
[6] F. Schüth, W. Schmidt, *Adv. Mater.* **2002**, *14*, 629 – 638.
[7] Q. Huo, D. Zhao, J. Feng, J. Kim, Y. Han, G. D. Stucky, *Chem. Mater.* **1999**, *11*, 2668.
[8] K. Yu, X. Wu, C. J. Brinker, J. Ripmeester, *Langmuir* **2003**, *19*, 7282.
[9] P. Falcaro, S. Costacurta, G. Mattei, H. Amenitsch, A. Marcelli, M. C. Guidi, M. Piccinini, A. Nucara, L. Malfatti, T. Kidchob, P. Innocenzi, *J. Am. Chem. Soc.* **2005**, *127*, 3838.
[10] S. Che, A. E. Garcia-Bennett, T. Yokoi, K. Sakamoto, H. Kunieda, O. Terasaki, T. Tatsumi, *Nat. Mater.* **2003**, *2*, 801 – 806.
[11] A. E. Garcia-Bennett, K. Miyasaka, S. Che, O. Terasaki, *Chem. Mater.* **2004**, *16*, 3597 – 3605.
[12] S. Che, Z. Liu, T. Ohsuna, K. Sakamoto, O. Terasaki, T. Tatsumi, *Nature* **2004**, *429*, 281 – 284.
[13] A. E. Garcia-Bennett, S. Che, T. Tatsumi, O. Terasaki, *Chem. Mater.* **2004**, *16*, 813 – 821.
[14] S. Kamiya, H. Tanaka, S. Che, T. Tatsumi, O. Terasaki, *Solid State Sci.* **2003**, *5*, 197 – 204.
[15] K. Hiraga, D. Shindo, M. Hirabayashi, O. Terasaki, D. Watanabe, *Acta Crystallogr.* **1980**, *36*, 2550 – 2554.
[16] X. Zeng, G. Ungar, Y. Liu, V. Percec, A. E. Dulcey, J. K. Hobbs, *Nature* **2004**, *428*, 157.
[17] Y. Sakamoto, M. Kaneda, O. Terasaki, D. Zhao, J.-M. Kim, G. D. Stucky, H. J. Shin, R. Ryoo, *Nature* **2000**, *408*, 449.
[18] R. P. Hodgkins, A. E. Garcia-Bennett, P. A. Wright, *Microporous Mesoporous Mater.* **2005**, *79*, 241 – 252.
[19] T. Yokoi, H. Yoshitake, T. Tatsumi, *J. Mater. Chem.* **2004**, *14*, 951 – 957.

